J|A|C|S
ARTICLES
Published on Web 11/25/2004

In Situ Raman Spectroscopy of Bias-Induced Structural Changes in Nitroazobenzene Molecular Electronic Junctions

Aletha M. Nowak and Richard L. McCreery*

Contribution from the Department of Chemistry, The Ohio State University, 100 West 18th Avenue, Columbus, Ohio 43210

Received July 14, 2004; E-mail: mccreery.2@osu.edu

Abstract: Carbon/nitroazobenzene (NAB)/titanium/gold molecular electronic junctions with active thicknesses of 7−8 nm were constructed having partially transparent Ti/Au top contacts, which permitted in situ monitoring of molecular structure with Raman spectroscopy for applied biases between +3 and −3 V. Deposition of the Ti/Au top contacts resulted in spectral changes similar to those accompanying NAB reduction in a conventional spectroelectrochemical experiment. Upon application of +3 V (carbon relative to Ti), the spectrum indicated reoxidation of the NAB reduction product, and this redox cycle could be repeated at least three times. When a voltage excursion to −2 or −3 V occurred, the spectra indicated irreversible loss of the nitro group, and a dramatic but reversible decrease in Raman intensity over the entire shift range examined. Negative applied voltage causes formation of reduced NAB and a high oxidation state of titanium, while positive voltage forms oxidized NAB and injects electrons into the titanium oxide layer. The spectral changes were correlated with current/voltage curves in order to probe the mechanism of rectification and conductance switching reported previously. Overall, the combination of spectroscopic and voltammetric results implies a conduction mechanism involving both NAB and titanium oxide, possibly mediated by the injection of carriers into the semiconducting titanium oxide, or by reduction of an insulating titanium oxide to a more conductive form.

Introduction

Significant research effort has been invested toward understanding metal/molecule/metal molecular junctions, due to the interesting and possibly valuable properties of molecules as components in electronic circuits.[1,2] Such characteristics may include negative differential resistance,[3] rectification,[4−7] conductance switching,[8−10] and photocurrent.[11−14] Molecular junction designs reported to date range from single-molecule junctions in scanning tunneling microscopy experiments or break junctions,[15−18] to monolayer junctions consisting of many molecules oriented in parallel between metallic or semiconducting contacts.[19−24] The nanometer size of such junctions in at least one dimension makes them difficult to probe by spectroscopic techniques that provide information about molecular structure. Furthermore, the generally opaque metallic contacts prevent characterization of molecular junctions with optical spectroscopy, even those with monolayer sensitivity. The current investigation was undertaken to provide in situ vibrational spectra of working molecular junctions under the influence of an applied voltage.

A popular junction fabrication approach involves self-assembled organothiolate monolayers (SAMs) on gold substrates[3,6,22−25] or Langmuir−Blodgett (L−B) films[4,5,9] with

(1) McCreery, R. *Chem. Mater.* **2004**, *16*, 4477.
(2) McCreery, R. *Special Issue: Molecular Electronics, The Electrochemical Society Interface* **2004**, *13*, 46.
(3) Chen, J.; Reed, M. A.; Rawlett, A. M.; Tour, J. M. *Science* **1999**, *286*, 1550.
(4) Metzger, R. M.; Chen, B.; Hopfner, U.; Lakshmikantham, M. V.; Vuillaume, D.; Kawai, T.; Wu, X.; Tachibana, H.; Hughes, T. V.; Sakurai, H.; Baldwin, J. W.; Hosch, C.; Cava, M. P.; Brehmer, L.; Ashwell, G. J. *J. Am. Chem. Soc.* **1997**, *119*, 10455.
(5) Metzger, R. M.; Xu, T.; Peterson, I. R. *J. Phys. Chem. B* **2001**, *105*, 7280.
(6) Zhou, C.; Deshpande, M. R.; Reed, M. A.; Jones, L.; Tour, J. M. *Appl. Phys. Lett.* **1997**, *71*, 611.
(7) Ashwell, G. J.; Tyrrell, W. D.; Whittam, A. J. *J. Am. Chem. Soc.* **2004**, *126*, 7102.
(8) Ranganathan, S.; Steidel, I.; Anariba, F.; McCreery, R. L. *Nano Lett.* **2001**, *1*, 491.
(9) Collier, C. P.; Wong, E. W.; Belohradsky, M.; Raymo, F. M.; Stoddart, J. F.; Kuekes, P. J.; Williams, R. S.; Heath, J. R. *Science* **1999**, *285*, 391.
(10) Ramachandran, G. K.; Hopson, T. J.; Rawlett, A. M.; Nagahara, L. A.; Primak, A.; Lindsay, S. M. *Science* **2003**, *300*, 1413.
(11) Velez, M.; Mukhopadhyay, S.; Muzikante, I.; Matisova, G.; Vieira, S. *Langmuir* **1997**, *13*, 870.
(12) Delaire, J. A.; Nakatani, K. *Chem. Rev.* **2000**, *100*, 1817.
(13) Matisova, G.; Markava, E.; Muzikante, I.; Fonavs, E.; Gerca, L. *Adv. Mater. Opt. Electron.* **1996**, *6*, 279.
(14) Matsumoto, M.; Terrettaz, S.; Tachibana, H. *Adv. Colloid Interface Sci.* **2000**, *87*, 147.
(15) Cui, X. D.; Primak, A.; Zarate, X.; Tomfohr, J.; Sankey, O. F.; Moore, A. L.; Moore, T. A.; Gust, D.; Harris, G.; Lindsay, S. M. *Science* **2001**, *294*, 571.
(16) Xiao, X.; Xu, B.; Tao, N. J. *Nano Lett.* **2004**, *4*, 267.
(17) Fan, F.-R. F.; Lai, R. Y.; Cornil, J.; Karzazi, Y.; Brédas, J.-L.; Cai, L.; Cheng, L.; Yao, Y.; David W. Price, J.; Dirk, S. M.; Tour, J. M.; Bard, A. J. *J. Am. Chem. Soc.* **2004**, *126*, 2568.
(18) Reed, M. A.; Zhou, C.; Muller, C. J.; Burgin, T. P.; Tour, J. M. *Science* **1997**, *278*, 252.
(19) Jaiswal, A.; Amaresh, R. R.; Lakshmikantham, M. V.; Honciuc, A.; Cava, M. P.; Metzger, R. M. *Langmuir* **2003**, *19*, 9043.
(20) Wang, W.; Lee, T.; Kamdar, M.; Reed, M. A.; Stewart, M. P.; Hwang, J.-J.; Tour, J. M. *Superlattices Microstruct.* **2003**, *33*, 217.
(21) Stapleton, J. J.; Harder, P.; Daniel, T. A.; Reinard, M. D.; Yao, Y.; Price, D. W.; Tour, J. M.; Allara, D. L. *Langmuir* **2003**, *19*, 8245.
(22) Slowinski, K.; Majda, M. *J. Electroanal. Chem.* **2000**, *491*, 139.
(23) Holmlin, R. E.; Haag, R.; Chabinyc, M. L.; Ismagilov, R. F.; Cohen, A. E.; Terfort, A.; Rampi, M. A.; Whitesides, G. M. *J. Am. Chem. Soc.* **2001**, *123*, 5075.
(24) Rampi, M. A.; Whitesides, G. M. *Chem. Phys.* **2002**, *281*, 373.

vapor-deposited metals as the top contact. While these approaches have revealed interesting electronic properties, the materials used do not lend themselves to spectroscopic characterization. The molecular origin of the electronic behavior of several of these devices has been questioned recently, and some of their behavior may be due to artifacts of fabrication, such as metal filaments between the contacts[26,27] or disruption of the Au−S bond.[10]

Recently we described an approach to fabricate molecular junctions using a flat graphitic carbon substrate (pyrolyzed photoresist film, PPF) and a titanium/gold top contact.[28] These junctions demonstrated reproducible electronic behavior and exhibited both rectification and conductance switching. Molecular layers are covalently bonded to the substrate by electrochemical reduction of aromatic diazonium ions in acetonitrile. A variety of molecules may be bound to the surface, including nitroazobenzene (NAB), azobenzene, biphenyl, terphenyl, nitrobiphenyl, and stilbene.[8,29] Through careful control of the deposition conditions, it is possible to produce molecular layers of variable thickness, as verified with atomic force microscopy (AFM) using a "scratching" technique.[30] In a previous report, the interactions between Ti and NAB-modified PPF surfaces were characterized with Raman and X-ray photoelectron spectroscopy (XPS).[31] Upon Ti deposition onto an NAB layer on PPF, the intensities of NAB modes associated with the NO_2 group decrease significantly, and XPS indicated formation of a Ti−N bond. These results provide evidence for a molecular junction with covalent bonding on both ends, with a C−C bond between the PPF substrate and NAB, and a Ti−N bond between NAB and Ti.[28,31] We later determined that the electronic behavior of the junctions depended strongly on the presence of titanium oxide, in that the junction resistance was much lower when the residual gas pressure was decreased during Ti deposition.[32,33] The spectroscopic effort described below was undertaken in part to determine if structural changes occurred in carbon/NAB/Ti junctions under an applied voltage, and to elucidate the role of both NAB and Ti oxides in determining the electronic properties of the carbon/NAB/Ti molecular junctions.

Optically transparent electrodes (OTE) have been used for several decades in electrochemistry, and more recently to probe conducting polymers in thin-film devices. A thin film of vapor-deposited metal may be sufficiently conductive to apply a bias while remaining ~50% transparent to UV−vis light. Thin-film OTEs were used by Kuwana et al.[34−38] to monitor solutions near an electrode surface, and by Friend et al.[39−41] on thin films of conducting polymers and organic light-emitting diodes. Hipps et al.[42,43] reported a Raman probe of an Al/Al oxide/phthalocyanine/Pb junction through a thin film of Pb, but did not observe changes in the Raman spectrum with applied bias. The current report describes an application of high-sensitivity Raman spectroscopy to carbon/NAB/Ti/Au molecular junctions, using a thin film of Ti and Au as an OTE. The results demonstrate structural rearrangement within the junction in response to an applied voltage.

Experimental Section

Pyrolyzed photoresist films (PPF) with an rms roughness <0.5 nm were prepared using established procedures.[44,45] Silicon wafers (boron doped, 12−16 Ω-cm) with a coating of 1500 Å of silicon nitride (Virginia Semiconductor, Inc.) were cut into 1 cm × 2.5 cm pieces and rinsed with acetone (Mallinckrodt AR, 99.7%), followed by isopropyl alcohol (Sigma-Aldrich, 99.5%), and then Nanopure water (18 MΩ-cm, Barnstead). The clean silicon nitride pieces were spin-coated with positive photoresist AZ P4330−RS (Clariant Corp.) and soft-baked at 90 °C for 20 min, and then cooled to room temperature before photolithography. A contact mask with an opaque 1 mm × 2 cm stripe was placed between the sample and the light source. A mercury arc lamp (Oriel Corp.) operating at 350 W was used to expose the photoresist for 120 s. The samples were submerged into the developer solution (AZ400K, Clariant Corp.) until the pattern was fully developed, about 2 min. After the samples were rinsed with nanopure water and dried with argon, pyrolysis was carried out as described previously at 1000 °C for 1 h in the presence of forming gas (95% nitrogen and 5% hydrogen).[28,45] The PPF samples were cleaned with acetonitrile (Sigma-Aldrich, 99.5%), which was treated with activated carbon,[46] and then filtered with 0.2-μm nylon filters (Millipore) prior to surface modification.

4-Nitroazobenzene 4′-diazonium tetrafluoroborate salts were prepared as previously described.[47−50] Electrochemical derivatization took place in an acetonitrile solution with 1 mM NAB diazonium salt and 0.1 M tetrabutylammonium tetrafluoroborate ($TBABF_4$, Aldrich, 99%) as the background electrolyte, and the solution was purged with argon for 20 min before derivatization. The Ag/Ag^+ reference electrode (0.01 M $AgNO_3$ and 0.1 M $TBABF_4$ in acetonitrile) was calibrated against the $E_{1/2}$ for the oxidation of ferrocene in acetonitrile to yield a Ag^+/Ag potential of 212 mV vs aqueous SCE. A 4.5 nm thick NAB multilayer covalently bound to the PPF surface was deposited using four scans from +400 to −600 mV vs Ag^+/Ag[30] at 200 mV/s. Such multilayers have been shown to result from attack of an initial NAB monolayer by additional NAB radicals formed by diazonium reduction, thus forming a phenyl−phenyl bond.[30,51] Samples were rinsed with and stored in activated-carbon-treated acetonitrile until metal deposition.

After drying with argon, the NAB-modified PPF samples were loaded in an electron beam evaporator (Veeco, Telemark) described previously.[28] Titanium was deposited through a shadow mask at 0.03

(25) Chen, J.; Calvet, L. C.; Reed, M. A.; Carr, D. W.; Grubisha, D. S.; Bennett, D. W. *Chem. Phys. Lett.* **1999**, *313*, 741.
(26) Jaiswal, A.; Amaresh, R. R.; Lakshmikantham, M. V.; Honciuc, A.; Cava, M. P.; Metzger, R. M. *Langmuir* **2003**, *19*, 9043.
(27) Service, R. F. *Science* **2003**, *302*, 556.
(28) McCreery, R. L.; Dieringer, J.; Solak, A. O.; Snyder, B.; Nowak, A.; McGovern, W. R.; DuVall, S. *J. Am. Chem. Soc.* **2003**, *125*, 10748.
(29) Anariba, F.; McCreery, R. L. *J. Phys. Chem. B* **2002**, *106*, 10355.
(30) Anariba, F.; DuVall, S. H.; McCreery, R. L. *Anal. Chem.* **2003**, *75*, 3837.
(31) Nowak, A. M.; McCreery, R. L. *Anal. Chem.* **2004**, *76*, 1089.
(32) McGovern, W. R.; Anariba, F.; McCreery, R. *J. Electrochem. Soc.*, in press.
(33) McCreery, R.; Dieringer, J.; Solak, A. O.; Snyder, B.; Nowak, A. M.; McGovern, W. R.; DuVall, S. *J. Am. Chem. Soc.* **2004**, *126*, 6200.
(34) Winograd, N.; Kuwana, T. *J. Electroanal. Chem* **1969**, *23*, 333.
(35) Winograd, N.; Blount, H. N.; Kuwana, T. *J. Phys. Chem.* **1969**, *73*, 3456.
(36) Blount, H. N.; Winograd, N.; Kuwana, T. *J. Phys. Chem.* **1970**, *74*, 3231.
(37) Winograd, N.; Kuwana, T. *J. Am. Chem. Soc.* **1970**, *92*, 224.
(38) Winograd, N.; Kuwana, T. *Anal. Chem.* **1971**, *43*, 252.
(39) Ziemelis, K. E.; Hussain, A. T.; Bradley, D. D. C.; Friend, R. H.; Ruhe, J.; Wegner, G. *Phys. Rev. Lett.* **1991**, *66*, 2231.
(40) Brown, T. M.; Friend, R. H.; Millard, I. S.; Lacey, D. J.; Butler, T.; Burroughes, J. H.; Cacialli, F. *J. Appl. Phys.* **2003**, *93*, 6159.
(41) Burroughes, J. H.; Jones, C. A.; Friend, R. H. *Nature* **1988**, *335*, 137.
(42) Hipps, K. W.; Dowdy, J.; Hoagland, J. J. *Langmuir* **1991**, *7*, 5.
(43) Hoagland, J. J.; Dowdy, J.; Hipps, K. W. *J. Phys. Chem.* **1991**, *95*, 2246.
(44) Ranganathan, S.; McCreery, R. L.; Majji, S. M.; Madou, M. *J. Electrochem. Soc.* **2000**, *147*, 277.
(45) Ranganathan, S.; McCreery, R. L. *Anal. Chem.* **2001**, *73*, 893.
(46) Ranganathan, S.; Kuo, T.-C.; McCreery, R. L. *Anal. Chem.* **1999**, *71*, 3574.
(47) Allongue, P.; Delamar, M.; Desbat, B.; Fagebaume, O.; Hitmi, R.; Pinson, J.; Saveant, J. M. *J. Am. Chem. Soc.* **1997**, *119*, 201.
(48) Delamar, M.; Hitmi, R.; Pinson, J.; Saveant, J. M. *J. Am. Chem. Soc.* **1992**, *114*, 5883.
(49) DuVall, S.; McCreery, R. L. *J. Am. Chem. Soc.* **2000**, *122*, 6759.
(50) Yang, H.-H.; McCreery, R. L. *J. Electrochem. Soc.* **2000**, *147*, 3420.
(51) Kariuki, J. K.; McDermott, M. T. *Langmuir* **2001**, *17*, 5947.

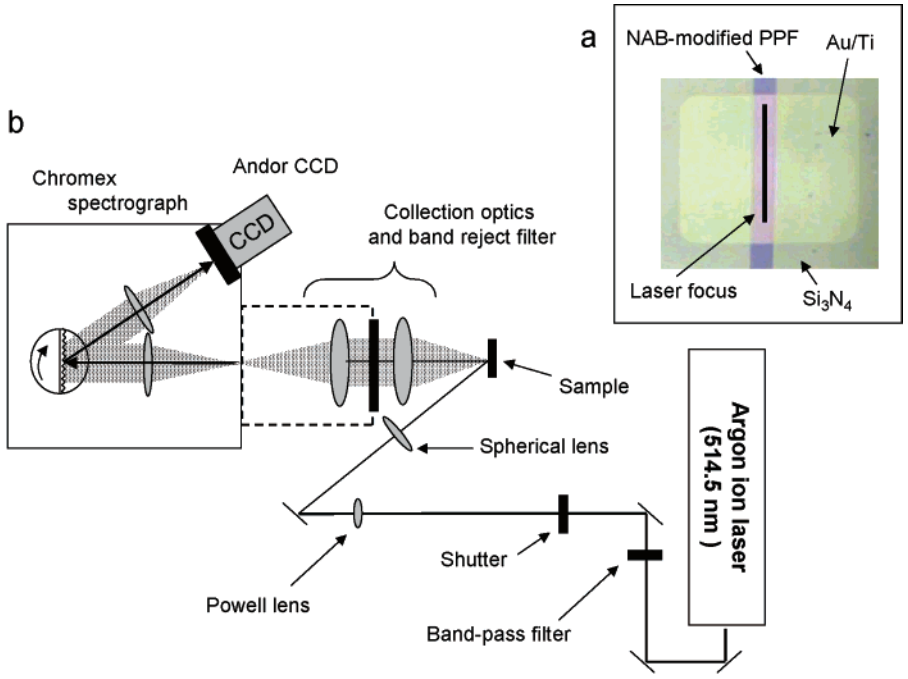

Figure 1. (a) Photograph of PPF/NAB(4.5)/Ti(1.0) junction with a transparent Ti(1.0)/Au(9.0) top contact. The PPF strip is 1 mm wide, and the laser line focus is 5 mm long. (b) Optical layout of laser, sample, and CCD spectrograph.

nm/s followed by Au at 0.1 nm/s, without breaking vacuum, thereby producing a PPF/NAB/Ti/Au molecular electronic junction. Metal thickness was measured in situ by a quartz crystal microbalance, and the pressure of the chamber was less than 2.7×10^{-6} Torr during metal deposition. To maintain optical transparency, the total thickness of the metal top contact was limited to 10.0 nm. The transparency of the metal top contact on quartz was measured with a UV−vis spectrometer (Perkin-Elmer Lambda 900). Over the wavelength range of 535−575 nm used for Raman spectroscopy, the transparencies of the Au(9.0)/Ti(1.0), Au(7.0)/Ti(3.0), and Au(5.0)/Ti(5.0) top contacts were 62.9−63.5%, 41.8−41.7%, and 28.9−28.7% versus a quartz plate, respectively. All junctions were allowed to "age" in air for approximately 6 days prior to analysis, since a previous investigation showed that a similar period was required to reach a constant Raman spectrum.[31] In addition to the partial reoxidation of the NAB reduced by titanium deposition reported previously,[31] exposure to air slowly oxidizes the disordered Ti oxide deposit.[32]

A photograph of a finished junction is shown in Figure 1a. The junction area is defined by the intersection of the NAB-modified PPF strip (1 mm wide) and the Au/Ti top contact (0.7 cm square), for a junction area of 0.07 cm^2. Electrical contact was made with alligator clips attached to an unmodified PPF pad (not shown) and the metal overlayer to the side of the junction. This geometry permits electrical contact without blocking the laser or scattered light.

Raman spectra were collected with a custom-built line-focused *f*/2 Raman spectrometer (Chromex) and a back-thinned CCD (Andor), described previously.[52] A diagram of the optical arrangement and Raman spectrometer is shown in Figure 1b. A 514.5 nm argon ion laser (Coherent) had a power of 30 mW at the sample. The focal line was approximately 5 mm × 50 μm, and had a relatively flat intensity profile due to the Powell lens.[52] The incidence angle of the laser was ~45° relative to the surface normal, and the laser electric field was polarized parallel to the long axis of the focal line. The Andor CCD (256 × 1024 pixels) was thermoelectrically cooled to −85 °C, and all spectra shown are averages of 10 integrations with durations of 2 s each. Spikes in the spectra were removed by comparing successive spectra and rejecting single points with intensities that exceeded those in the previous spectrum by more than 200 CCD digitizer units. A linear baseline correction was applied to all spectra, and peak center frequencies were measured using the "center X" function in Grams 32/AI, version 6.00 (Galactic Industries, Salem, NH). Peak intensities were determined as peak height above this linear baseline. The Raman shift axis was calibrated with benzonitrile, and intensities were not corrected for instrument response. In all spectra shown, the spectrum of PPF obtained under the same conditions was subtracted, with its intensity adjusted so the subtracted spectrum had a 1595 cm^{-1} band undistorted by a residual G band from the PPF.

Current−voltage measurements were performed with custom electronics based on LabView (National Instruments, 6111 DAQ board, 12 bit), and potential pulses were applied with a commercial potentiostat (Epsilon, Bioanalytical Systems). All measurements were conducted at room temperature (22−24 °C). When the applied potential is positively biased (PPF relative to Ti), a positive current corresponds to transport of electrons through the junction from Ti to PPF. To test the integrity of each new junction, the low-voltage resistance and 3 V scans were measured. Junctions exhibiting a linear dependence on voltage over ±3 V and low resistance less than 1000 Ω (about 10% of all samples) were rejected from further study. Samples exhibiting nonlinear current−voltage characteristics were subjected to a series of potential pulses during which Raman spectra were collected. The PPF/NAB/Ti/Au junctions were allowed to equilibrate at a given potential for 30 s prior to spectrum acquisition, and the potential was held until integration was complete (an additional ~25 s).

Results

To clearly indicate the titanium thickness, junctions will be identified in the format PPF/NAB(4.5)/Ti(1.0), with numbers in parentheses indicating thickness in nanometers, and all junctions had a protective Au outer layer for a total metal thickness of 10.0 nm. Carbon-based molecular electronic junctions incorporating an organic layer of chemisorbed NAB with a Au/Ti top contact were chosen for this study due to the spectroscopic[53−55] and electronic[8,28,33,56] characterization reported previously, as well as the large Raman cross section of

(52) Ramsey, J. D.; Ranganathan, S.; Zhao, J.; McCreery, R. L. *Appl. Spectrosc.* **2001**, *55*, 767.

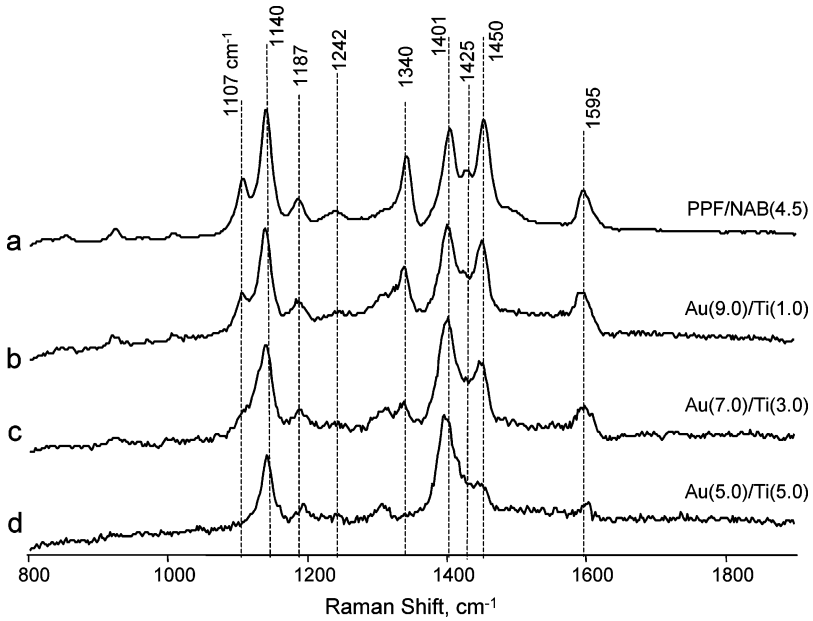

Figure 2. Raman spectra of PPF/NAB(4.5) surfaces before (a) and after (b−d) deposition of top contact. These and all other Raman spectra are averages of 10 2-s CCD integrations, and an unmodified PPF spectrum was subtracted.

NAB. The 4.5 nm NAB film plus 1−3 nm of Ti yielded an active junction thickness of 5.5−7.5 nm. Figure 2 shows the Raman spectrum for PPF/NAB without the metal top contact (Figure 2a), as well as spectra collected from junctions following deposition with various Au/Ti thicknesses. In all cases shown in Figure 2, the spectra were obtained at open circuit, in the absence of an applied voltage. In a previous study, Raman and XPS spectra were collected[31] from NAB-modified PPF surfaces after deposition of 1.0 nm of Ti but no Au. The spectrum observed for the Au(9.0)/Ti(1.0) top contact is very similar to what was reported previously for Ti(1.0) alone, indicating that the additional Au deposition does not apparently alter the NAB layer. After deposition of the Au/Ti top contact, a significant decrease in the intensity of the 1107, 1340, and 1450 cm^{-1} peaks is observed (Figure 2b−d), which is progressively greater as the Ti thickness increases. These peaks are associated with normal modes involving the NO_2 group, specifically the NO_2 stretch (1340 cm^{-1}), the phenyl−NO_2 stretch (1107 cm^{-1}), and a N═N vibration coupled to NO_2 (1450 cm^{-1}).[31,55] Similar spectra were obtained when the metal was deposited at lower residual gas pressure (~4.0×10^{-7} Torr). Peak frequencies and normal-mode assignments for the peaks apparent in Figure 2 are listed in Table 1.

Figures 3 and 4 illustrate the spectroscopic effects of application of +3 V pulses to NAB junctions (PPF +3 V relative to Ti/Au). An initial spectrum acquired with an applied voltage of +0.05 V was indistinguishable from that obtained at open circuit, for either 1.0 or 3.0 nm thicknesses of Ti. The spectra shown in Figure 3b,d were obtained after junctions were held at +3 V for a total of 270 s. Changes were observed in the relative intensity of the peaks assigned to the azo stretches (1401 and 1450 cm^{-1}) for both junctions, whereas other bands were not significantly affected by the application of a positive voltage.

Table 1. Raman Peak Frequencies and Assignments for Nitroazobenzene on PPF

free NAB in CCl_4	Ti(1.0)/ NAB(4.5)	Ti(3.0)/ NAB(4.5)	calcd for 4′-phenyl-NAB[a]	assignment[b,c]
1112	1107 ± 0.9	1107 ± 1.3	1086 (59)	phenyl−NO_2 stretch and C−H wag
1147	1140 ± 0.7	1141 ± 0.7	1127 (62)	phenyl−NN stretch
1183	1187 ± 1.3	1192 ± 3.2	1172 (65)	CH bend
	1242 ± 2.3	1243 ± 3.3	1247 (68)	phenyl−NAB stretch
1347	1340 ± 0.9	1340 ± 1.7	1337 (74)	NO_2 stretch
1412	1401 ± 1.0	1399 ± 1.9	1394 (76)	N═N stretch + ring A
	1425 ± 1.8			
1449	1450 ± 1.0	1449 ± 1.6	1454 (79)	N═N stretch
1470			1472 (80)	phenyl−N═N stretch + ring deformation
1492			1498 (82)	phenyl−N═N stretch + ring deformation
1594	1595 ± 2.9	1597 ± 3.4	1589 (86)	CC ring stretch

[a] Mode number is in parentheses, Gaussian 98, B3LYP/6-31G(d). [b] Ring A = phenyl group with NO_2 group; ring B = phenyl group without NO_2 group. [c] See refs 31, 55, and 63.

The ratio (R) of the peak intensity of the 1401 cm^{-1} to the 1450 cm^{-1} peak measured at +3 V is reproducibly smaller than the value at +0.05 V. The intensity ratios at +0.05, +1, +2, and +3 V are plotted in Figure 4, along with the ratio for PPF/NAB without the metal top contact. For PPF/NAB(4.5)/Ti(1.0) and PPF/NAB(4.5)/Ti(3.0) junctions, the azo peak intensity ratio decreases steadily from +0.05 V to +3 V. The ratio reaches an equilibrium value for the PPF/NAB(4.5)/Ti(1.0) junction during the first +3 V pulse, which is less than the ratio observed for PPF/NAB with no metal applied. For PPF/NAB(4.5)/Ti(3.0), the ratio continues to decrease with subsequent +3 V pulses and approaches the values measured for PPF/NAB before metal deposition.

Figures 5−7 show the effect of a positive potential excursion on fresh NAB junctions in more detail. For the spectra shown in Figure 5, the indicated voltage was imposed on a PPF/NAB-(4.5)/Ti(1.0) junction for 30 s, and then continued during an

(53) Liu, Y.-C.; McCreery, R. L. *Anal. Chem.* **1997**, *69*, 2091.
(54) Liu, Y.-C.; McCreery, R. L. *J. Am. Chem. Soc.* **1995**, *117*, 11254.
(55) Itoh, T.; McCreery, R. L. *J. Am. Chem. Soc.* **2002**, *124*, 10894.
(56) Solak, A. O.; Ranganathan, S.; Itoh, T.; McCreery, R. L. *Electrochem. Solid State Lett.* **2002**, *5*, E43.

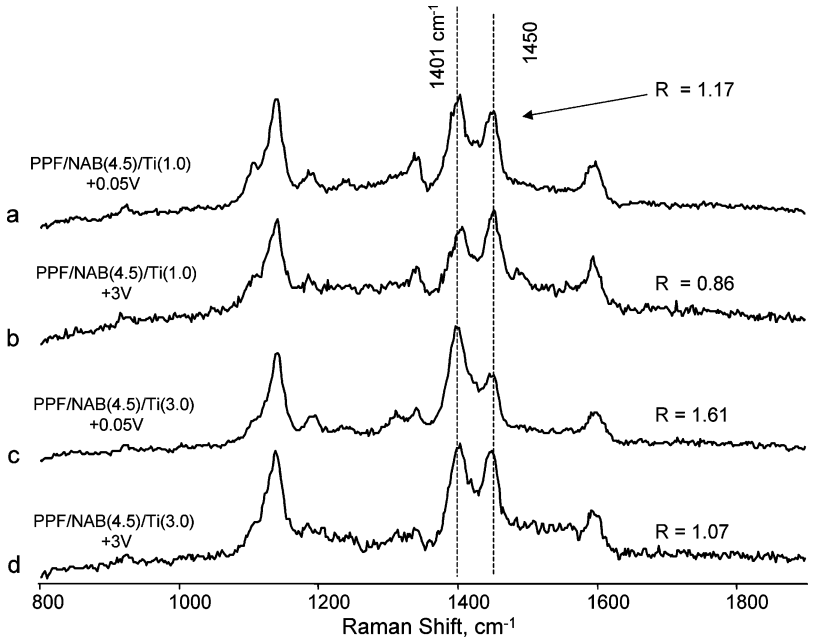

Figure 3. Raman spectra of PPF/NAB(4.5) junctions with an applied bias voltage. Spectra b and d were acquired after a total of 270 s at +3 V (PPF relative to Ti). *R* is the ratio of peak intensities for the 1401 and 1450 cm^{-1} bands, measured relative to baseline.

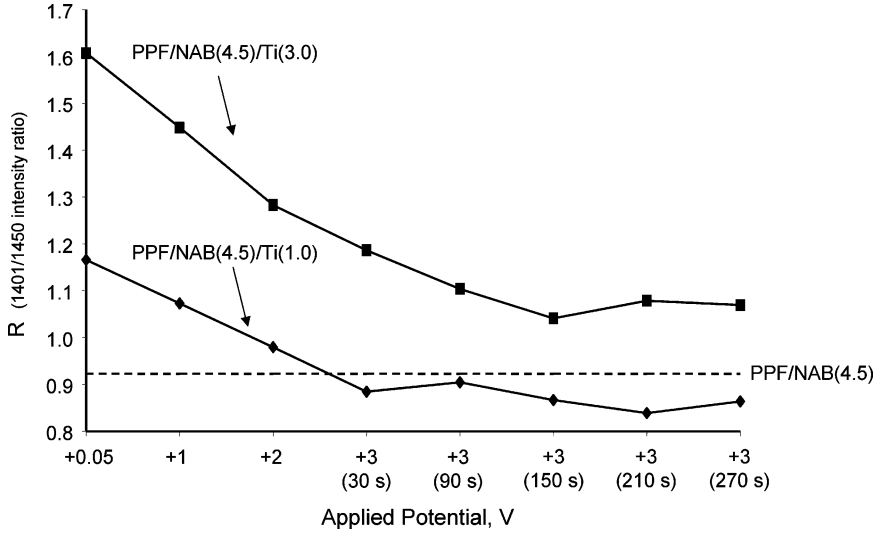

Figure 4. Trend of 1401/1450 intensity ratio (*R*) with applied bias and time. *X*-axis labels indicate both voltage and time. Dashed line is the *R* observed before Ti/Au deposition.

additional 30 s of spectrum acquisition. This process was repeated for progressively more positive voltages, and then returned to +0.05 V after reaching +3 V. The intensity changes observed for the +0.05 V to +3 V excursion (Figure 5a−d) are not immediately reversible, in that return to +0.05 V (Figure 5e) does not return the 1401/1450 ratio to its original value of ∼1.1. However, a negative voltage excursion to −1 V does "reset" the spectrum to its original appearance. As shown in Figure 6, qualitatively similar behavior was observed for the PPF/NAB(4.5)/Ti(3.0) junction, although the 1401/1450 ratio started at a higher value (∼1.5 vs ∼1.1). Figure 7 shows that the progression of decreasing 1401/1450 ratios is repeatable for at least three voltage cycles, as was the "reset" observed at −1 V. In a few cases not shown, junctions which experienced a +3 V applied voltage and returned to +0.05 V slowly "reset" without a −1 V excursion, but the spectral changes were much slower at +0.05 V (>1 h) than at −1 V (<30 s.).

When the applied voltage was extended to values negative of −1 V, the spectral changes observed for PPF/NAB(4.5)/Ti(1.0) junctions were more dramatic (Figure 8). Three changes in the spectra can be observed at −2 and −3 V. First, the intensity ratio of the 1401 cm^{-1} peak to the 1450 cm^{-1} peak increases above its initial value of ∼1.1, to approximately 2.0. Second, at −2 V the spectrum shows a significant decrease in the intensity of the peaks at 1107 and 1340 cm^{-1}, which have been assigned to the phenyl−NO_2 and NO_2 stretches, respectively. The intensity of these peaks did not recover by returning to positive potentials, although roughly half of the junctions examined showed a partial recovery of these bands over a period of one month in air at open circuit. Finally, the intensity of the entire spectrum decreased upon a voltage excursion to −3 V (Figure 8d). As shown in Figure 8e, the intensities of the 1140, 1401, 1450, and 1595 cm^{-1} bands rapidly returned to nearly their initial magnitudes upon return to +0.05 V. Both the 1.0

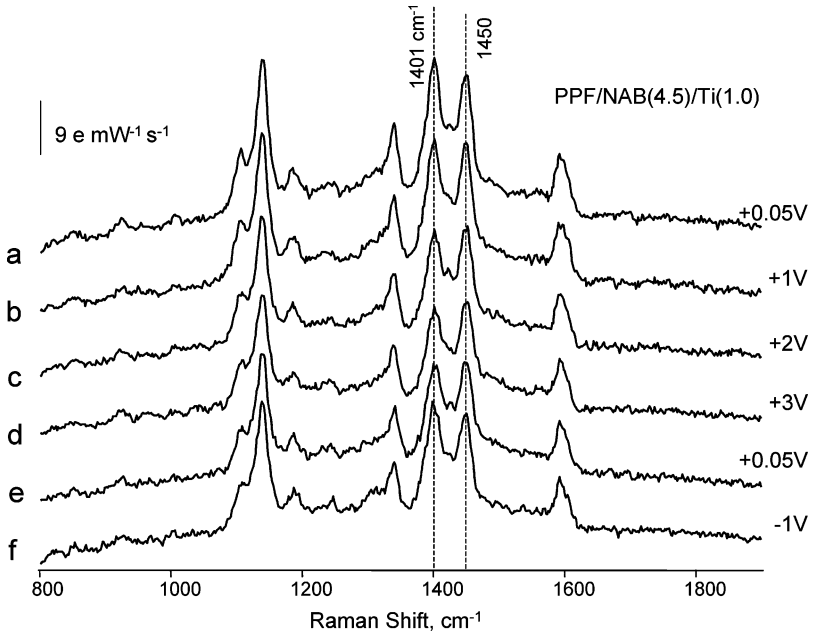

Figure 5. Spectra of PPF/NAB(4.5)/Ti(1.0) junction obtained at the indicated bias voltages. The junction was held for 30 s at each voltage, and bias was kept on during an additional 30 s for spectrum acquisition. Scale bar indicates photoelectrons collected at the CCD, normalized for integration time and laser power. Spectra were acquired in the order shown, from top to bottom.

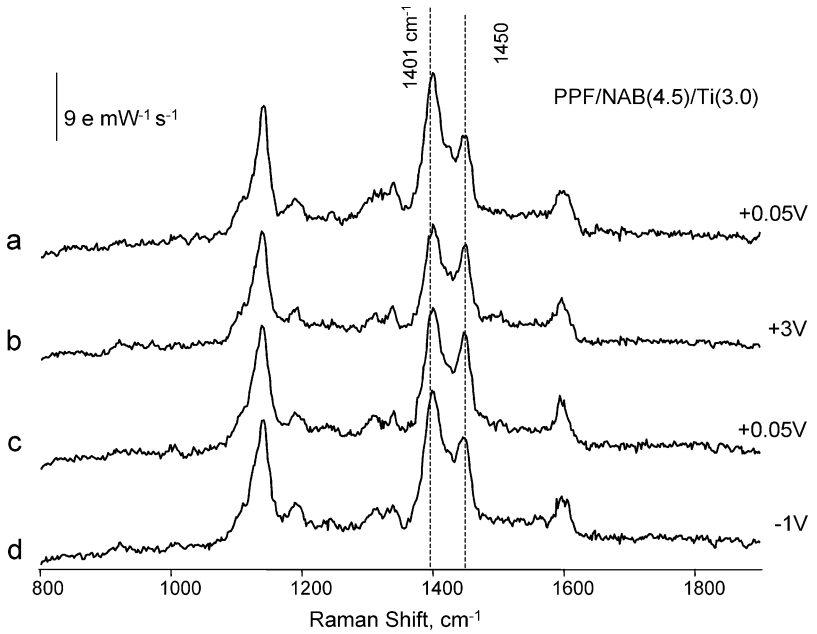

Figure 6. Raman spectra of a PPF/NAB(4.5)/Ti(3.0) junction during the same sequence of bias voltages used for Figure 5. Four of the six spectra are shown for clarity.

nm Ti junctions (Figure 8) and 3.0 nm Ti junctions showed similar reversible decreases in Raman intensity upon excursions to −3 V. The trend in relative peak intensities with voltage is summarized in Table 2 for three voltage excursions between −1 and +3 V. Table 3 summarizes the behavior of four Ti-(1.0) junctions following a −3 V voltage excursion, showing both the irreversible loss of the NO_2 features and the dynamics of the 1401 and 1450 cm^{-1} bands upon return to +3 V.

The *i*/*V* curves for NAB junctions with 3.0 nm of Ti were similar to those reported earlier for much thicker Ti top contacts.[28] Figure 9a shows that the strong rectification reported earlier persists for ∼100 scans at 1 V/s, but begins to degrade thereafter. The first 10 scans, which include the time period over which the spectra in Figures 5−7 were collected, are indistinguishable. At faster scan rates (Figure 9b), hysteresis is apparent in the *i*/*V* curves for voltages negative of −1 V, as observed previously.[28] Current vs time transients were similar to those reported previously, with the current reaching a constant value within about 10 s after a voltage change. A +3 V pulse results in >1 mA currents, while a −3 V pulse yields a much smaller current (∼1 μA) after a brief negative transient. All Raman spectra were obtained after voltage pulses lasting 30 s, hence in a region where the current had reached a constant value.

The distinct Raman spectra at +0.05, +3, and −3 V in Figures 5 and 8 imply different molecular structures at each bias voltage. To correlate the spectra with the *i*/*V* characteristics, fast voltage scans were performed after holding the bias for 60 s at +3 or −3 V. Figure 10 shows *i*/*V* curves (100 V/s) initiated

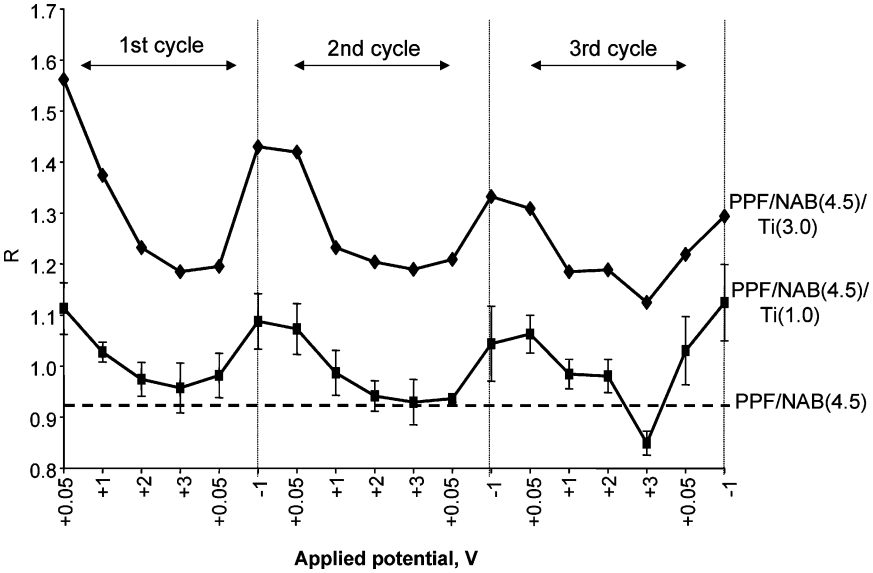

Figure 7. 1401/1450 intensity ratio as a function of bias for three voltage cycles similar to that shown in Figure 5. Dashed line is for PPF/NAB without a metal top contact. Error bars on NAB(4.5)/Ti(1.0) plot represent ±1 standard deviation for four independent samples. Upper plot is the average of four NAB(4.5)/Ti(3.0) samples. Note that the *X*-axis is labeled with the applied voltage, in order from left to right.

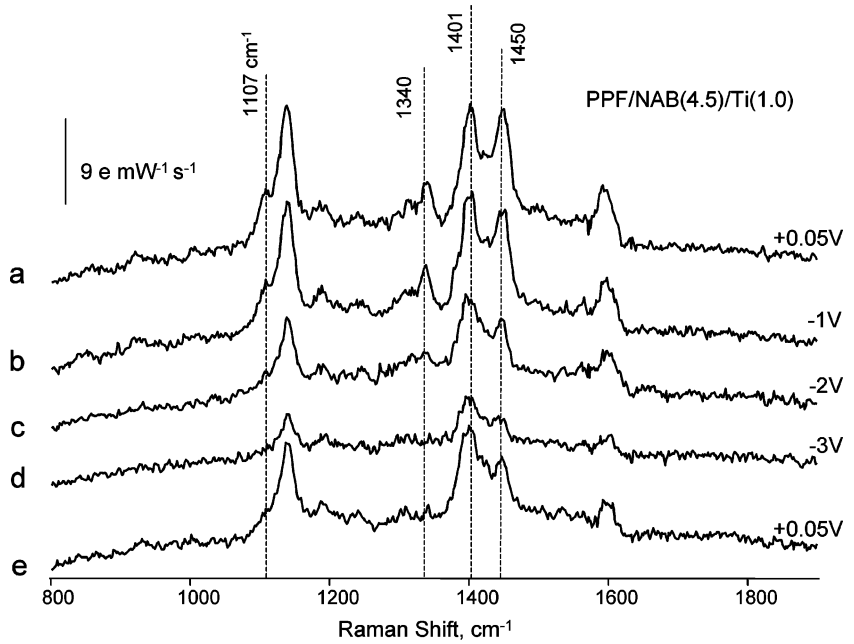

Figure 8. Raman spectra for PPF/NAB(4.5)/Ti(1.0) junction during an excursion to negative bias. All spectra are on the same intensity scale, but are offset for clarity.

at 0.05, +3, and −3 V obtained immediately after a 60-s hold at the indicated potential. The +3 V pulse yielded an *i*/*V* curve with the largest current magnitudes and also the largest hysteresis at negative *V*. The −3 V pulse yielded very small currents at negative *V*, and reduced current at +3 V. Superimposed in Figure 10 are the Raman spectra obtained at the indicated initial voltage, immediately before the voltage scan.

The NAB samples with 1.0 nm of Ti and 9.0 nm of Au exhibited some of the same changes in the *i*/*V* curves as those for 3.0 nm of Ti, but somewhat smaller in magnitude. Figure 11 shows *i*/*V* curves (10 V/s) initiated at 0 V following +3 and −3 V pulses lasting 60 s. As was the case for Ti(3.0), the current following a −3 V pulse was smaller in magnitude at both potential limits, but the rectification was weaker than the case for the thicker Ti layer. Control junctions were prepared for both thicknesses of Ti, using an identical fabrication procedure but omitting the NAB deposition step. As shown in Figures 10 and 11, the control junctions showed linear *i*/*V* behavior which was independent of scan rate. The currents were much larger than those of the NAB junctions and showed no effect of polarization at +3 or −3 V. The mean resistances and standard deviations for four control junctions of each type were 665 ± 132 Ω for PPF/Ti(3.0)/Au and 558 ± 66 Ω for PPF/Ti(1.0)/Au, both measured at 100 V/s. The majority of this "background" resistance is due to the thin (∼2 μm) film of PPF, with its relatively high resistivity (5 mΩ-cm).[44]

Discussion

The primary conclusions permitted by the spectroscopic results are the unequivocal evidence for bias-induced structural

Table 2. Peak Intensity Ratios for PPF/NAB(4.5)/Ti(1.0)/Au Junctions as Functions of Applied Voltage

voltage (V)	*I*(1340)/*I*(1450)	*I*(1401)/*I*(1450)
0.05	0.65 ± 0.04[a]	1.06 ± 0.05
1	0.67 ± 0.06	1.01 ± 0.02
2	0.63 ± 0.06	0.93 ± 0.03
3	0.62 ± 0.05	0.91 ± 0.05
0.05	0.61 ± 0.05	0.93 ± 0.04
−1	0.63 ± 0.04	1.08 ± 0.05
0.05	0.63 ± 0.03	1.03 ± 0.05
1	0.61 ± 0.02	0.97 ± 0.04
2	0.59 ± 0.05	0.90 ± 0.03
3	0.57 ± 0.07	0.87 ± 0.04
0.05	0.59 ± 0.05	0.93 ± 0.01
−1	0.59 ± 0.04	1.05 ± 0.07
0.05	0.60 ± 0.06	1.02 ± 0.04
1	0.55 ± 0.07	0.96 ± 0.03
2	0.56 ± 0.08	0.94 ± 0.03
3	0.56 ± 0.08	0.88 ± 0.02
0.05	0.54 ± 0.04	0.95 ± 0.07
−1	0.61 ± 0.03	1.07 ± 0.07
−2	<0.05	1.21 ± 0.07
−3	<0.05	1.26 ± 0.07
0.05	<0.05	1.22 ± 0.09

[a] Mean and standard deviation based on four samples

Table 3. Raman Peak Ratios for PPF/NAB(4.5)/Ti(1.0) Junctions before and after an Excursion to −3 V

voltage (V)	*I*(1340)/*I*(1450)	*R*(1401/1450)
0.05	0.65 ± 0.01[a]	1.05 ± 0.05
1	0.66 ± 0.03	1.02 ± 0.08
2	0.64 ± 0.03	0.98 ± 0.06
3	0.57 ± 0.06	0.94 ± 0.06
0.05	0.58 ± 0.04	0.94 ± 0.09
−1	0.59 ± 0.03	1.08 ± 0.03
−2	<0.05	1.30 ± 0.09
−3	<0.05	1.33 ± 0.14
0.05	<0.05	1.38 ± 0.13
3	<0.05	1.06 ± 0.09
0.05	<0.05	1.16 ± 0.14

[a] Mean and standard deviation based on four samples.

changes in the NAB molecular layer, their association with a redox process driven by the applied voltage, and the correlation of these structural changes with strong modulation of junction conductivity. These findings result from the direct probe of junction structure provided by in situ Raman spectroscopy. The combination of a sensitive Raman spectrometer, a strong NAB Raman cross section, and 28−64% transparent top contacts enables acquisition of the in situ Raman spectra shown in Figures 2, 3, 5, 6, and 8. NAB is preresonant at 514.5 nm, and bonding to the large π system of graphitic carbon further increases its Raman cross section.[53] As noted previously,[31,55] the Raman signal/noise ratio is sufficient to observe monolayers of NAB, although the 4.5 nm NAB films studied here represent a multilayer approximately three NAB molecules thick. Note also that neither PPF, Ti, nor Au supports electromagnetic field enhancement at 514.5 nm, so the strong Raman signal is due primarily to the high NAB/PPF cross section. Slow degradation of the Raman intensity with laser exposure is evident in Figure 7, and appears to result from photobleaching of NAB. The line focus used here has a power density approximately 3% that of a point focus with the same laser power,[52] making the line focus essential for reducing laser damage to an acceptable level.

The ratios of the 1401/1450 peak intensities indicated in Figures 2−7 are important indicators of NAB reduction. In a previously reported spectroelectrochemical experiment, an NAB monolayer chemisorbed to glassy carbon was monitored with Raman spectroscopy in an acetonitrile electrolyte.[55] Electrochemical reduction of chemisorbed NAB to its anion radical showed decreases in the intensities of bands at 1334 and 1444 cm^{-1}, and an increased intensity for a band at 1398 cm^{-1}. In terms of relative intensities, the ratio of the 1398/1444 intensities increased as NAB was reduced electrochemically. The in situ Raman spectra in PPF/NAB/Ti molecular junctions show variations in relative Raman intensity which are similar to the electrochemical case, with the increase in 1401/1450 ratio upon deposition of titanium indicating reduction of NAB by Ti atoms.

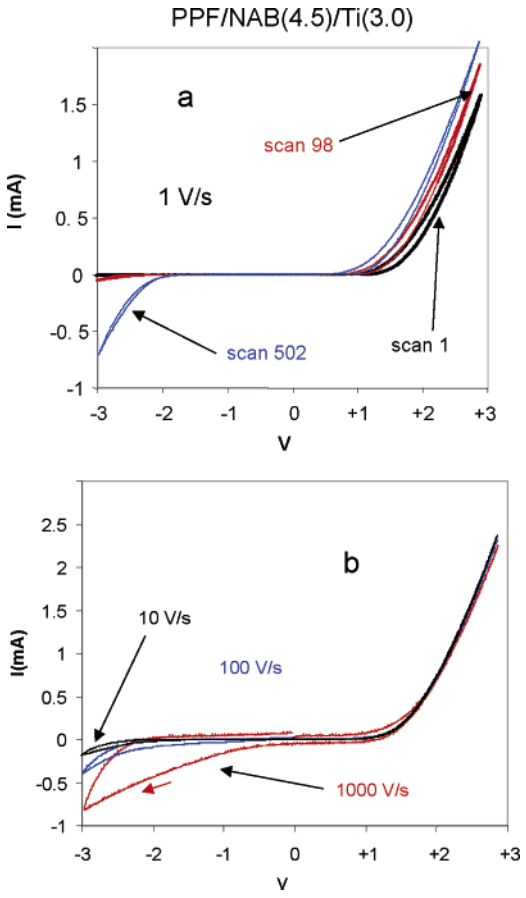

Figure 9. (a) Repetitive *i*/*V* scans for a PPF/NAB(4.5)/Ti(3.0) junction obtained at 1.0 V/s. Scans required 12 s each, with a 60-s hold at $V = 0$ between scans. (b) *i*/*V* curves at three scan rates for a fresh PPF/NAB-(4.5)/Ti(3.0) junction, initiated at $V = 0$ in a positive direction.

Although the changes in relative intensities for the +3 to −1 V range are not dramatic, they are reproducible from sample to sample and repeatable for a given sample (Figure 7, Table 2). Combined with the changes in 1107 and 1340 cm^{-1} intensities, the variations in the 1401/1450 intensity ratio provide unequivocal proof of a structural change in the NAB layer with variation in applied voltage. By analogy to the electrochemical investigation, loss of NO_2 features at 1107 and 1340 cm^{-1} and an increase in 1401/1450 are associated with reduction of NAB and accompanying loss of the NO_2 group Raman bands. For the electrochemical case, the NAB radical ion resulting from NAB reduction resembled a quinoid species with a weakened N═N bond and a rehybridized NO_2 group.[55] The observation of similar spectral changes in the in situ junction spectra of Figures 2, 3, and 5 indicates that NAB is reduced and oxidized within the junction depending on the applied bias. When the PPF is

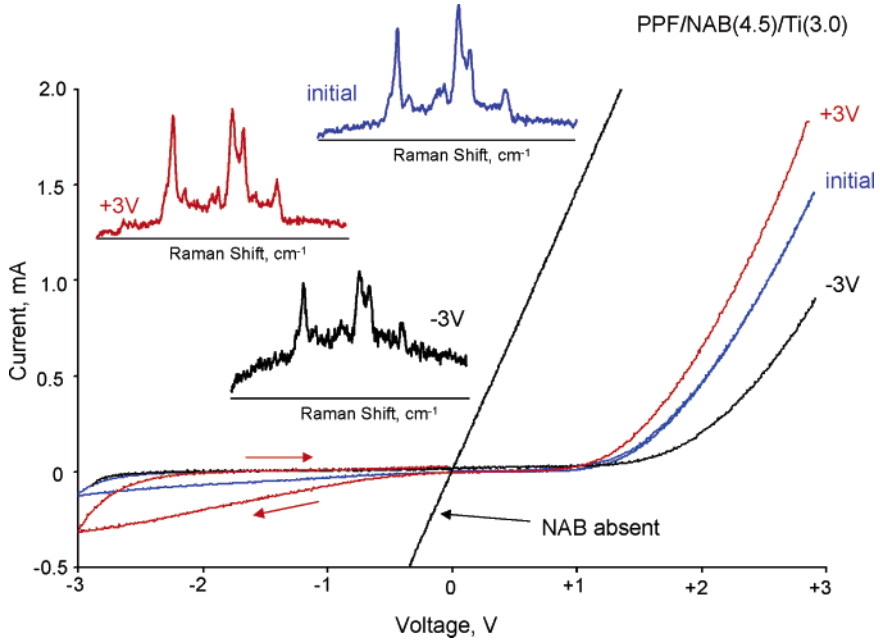

Figure 10. *i*/*V* curves (100 V/s) for a PPF/NAB(4.5)/Ti(3.0) junction initiated at $V = 0$ (labeled "initial") and after 60-s holds at $V = +3$ and -3 V. The latter two curves were initiated at the hold voltage. Raman spectra (with varying intensity scales) at each voltage appear as insets. The curve marked "NAB absent" was obtained with a control junction lacking NAB (PPF/Ti(3.0)/Au) at 100 V/s.

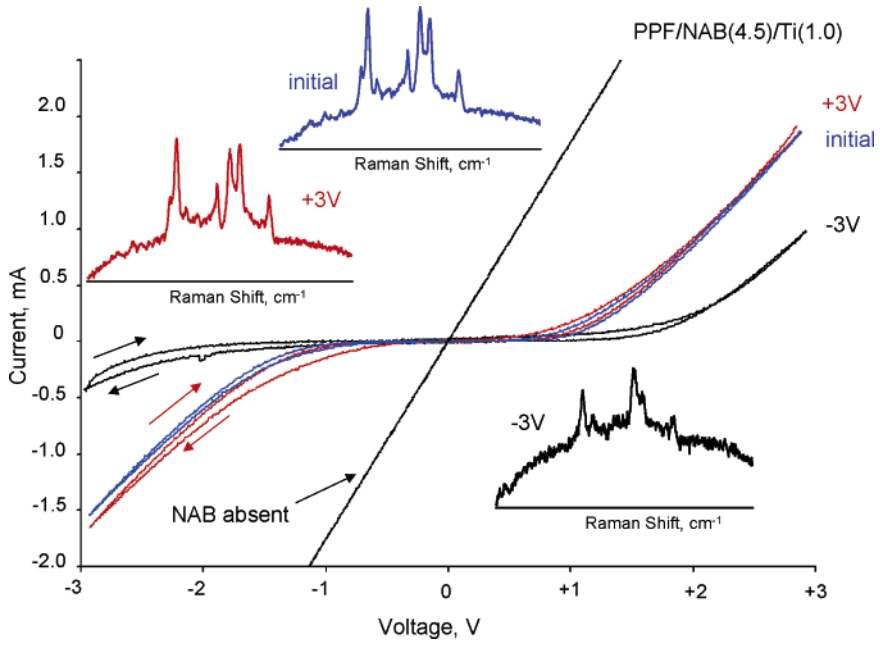

Figure 11. Same as Figure 10, but for a NAB(4.5) junction with 1.0 nm of Ti instead of 3.0 nm. Arrows show direction of hysteresis. The curve marked "NAB absent" was obtained with a control junction lacking NAB (PPF/Ti(1.0)/Au) at 100 V/s.

positive, NAB is oxidized and the 1401/1450 ratio decreases, while a -1 V bias with PPF negative increases the 1401/1450 intensity ratio. This apparent redox activity in a PPF/NAB/Ti junction shows similarities to the electrochemical case, but it is certainly distinct from conventional redox reactions in solution. The junction does not contain an intentional solvent or electrolyte, although ion motion involving the TiO_x layer or unknown impurities is conceivable. Hence the electrochemistry within the junction is more similar to solid-state redox cells involving a redox polymer or a polymeric electrolyte[57−59] than it is to a solution-phase redox cell.

The spectral variations shown in Figures 2−7 permit several conclusions about the effect of Ti and applied bias on NAB layer structure. First, e-beam-deposited Ti partially reduces NAB, with more extensive reduction observed for thicker Ti layers (Figure 2). A 5.0 nm layer of Ti was sufficient to decrease the NO_2 stretch intensity (1340 cm^{-1}) to a negligible level. Such a reduction is energetically reasonable, given the negative redox potential of Ti^{2+}/Ti (-1.6 V vs NHE) compared to NAB/NAB^- (-0.5 V vs NHE). Second, a positive bias of 3 V reoxidizes

(57) Murata, K.; Izuchi, S.; Yoshihisa, Y. *Electrochim. Acta* **2000**, *45*, 1501.
(58) Skotheim, T. A.; Florit, M. I.; Melo, A.; O'Grady, W. E. *Phys. Rev. B* **1984**, *30*, 4846.
(59) Reed, R. A.; Wooster, T. T.; Murray, R. W.; Yaniv, D. R.; Tonge, J. S.; Shriver, D. F. *J. Electrochem. Soc.* **1989**, *136*.

some or all of the reduced NAB, and the spectrum approaches that observed for PPF/NAB preceding metal deposition. Third, return to +0.05 V after a +3 V excursion did not restore the initial 1401/1450 ratio, implying that the NAB remains oxidized after the +3 V excursion. However, the NAB is rapidly reduced at −1 V to a spectrum resembling that before the +3 V excursion. All three observations are consistent with a dynamic, chemically reversible redox reaction between chemisorbed NAB and a reduced species resembling the radical ion observed electrochemically. The reaction is not controlled by a conventional electrode potential relative to a standard potential, but rather by an applied electric field. Apparently, the relaxation of the electric field when the bias is decreased from +3 V to +0.05 V is not sufficient to partially reduce NAB back to NAB^-, but a reverse bias at −1 V does restore the initial partially reduced junction.

Biases negative of −1 V for both 1.0 and 3.0 nm Ti junctions caused more dramatic changes in the Raman spectrum. At −2 or −3 V, the 1107 and 1340 cm^{-1} NO_2 features are irreversibly removed, and the entire spectrum has less than one-third of its initial intensity at +0.05 V. However, most of the intensity decrease is reversed upon return to +0.05 V. The reversible decrease in Raman intensity could be due to a shift in the absorption spectrum in the electric field, with an associated decrease in resonance enhancement. However, the irreversible loss of NO_2 Raman features implies a persistent structural change once the bias is negative of −1 V, which was not reversed even at +3 V. To account for all of the spectroscopic changes, a second redox pair must be invoked, which is formed irreversibly when NAB is reduced beyond the NAB/NAB^- couple, either by additional titanium or by very negative potentials. The structure of this second redox pair is unknown at present, but it does show a chemically reversible redox process similar to that described for NAB/NAB^-, but without the presence of a NO_2 group (Table 3). Under the hypothesis of a second redox pair, the 3.0 nm Ti deposit is sufficient to irreversibly remove some of the NAB/NAB^- from the junction, leading to the permanent offset of the 1401/1450 intensity ratio apparent in Figure 7, relative to the 1.0 nm case.

Given the existence of a field-driven structural rearrangement in the junction, several questions arise which will be considered in turn. First, when a positive bias removes electrons from the NAB/NAB^- layer, is there a corresponding electron injection at the $Au/Ti/TiO_x$ interface? Second, how do these apparent redox changes correlate with the junction conductivity shown in Figures 9−11? Third, is a field-driven electron transfer in a redox cell of <10 nm thickness at all similar to a conventional electrochemical redox reaction driven by the electric field in a double layer?

We reported elsewhere that the Ti deposit consists of mainly Ti^0, Ti^{II}, and Ti^{III} as disordered oxides and hydroxides,[32] as well as small amounts of TiO_2. The distribution of oxides changed slowly with time, with a gradual increase in Ti^{IV} content.[32] Furthermore, replacing Ti with Cu in PPF/NAB junctions resulted in much higher currents and little or no rectification.[32,33] Analogous optically transparent PPF/NAB/Cu/Au junctions with the configuration shown in Figure 1 were too conductive to study due to their large areas. For Ti junctions, an oxide deposit should be capable of accepting electrons to produce a lower Ti oxidation state. Such a process could be viewed as a traditional redox reaction with accompanying ion motion (e.g., of OH^- ion), or as electron injection into a conduction band to produce an accumulation layer with associated space charge. Leaving the issue of counterion motion an open question at present, both processes can be represented by reaction 1, with P representing an oxidation state of Ti:

$$NAB^- + Ti\ (P) \rightleftarrows NAB + Ti\ (P-1) \qquad (1)$$

Reaction 1 is driven to the right by a positive bias and to the left by a negative bias applied to the junction. As noted previously, the specifics of reaction 1 depend on what counterions are produced by the reactions between Ti atoms, residual gases, and NAB.[32] Furthermore, TiO and Ti_2O_3 are much more conductive than TiO_2, so a decrease in Ti oxidation state may cause a significant conductance change in the Ti oxide layer. According to a redox hypothesis, the electrons leaving NAB^- are injected into TiO_x, and electroneutrality is preserved for the entire cell. Whether the result is a conventional reduction of TiO_x, possibly to Ti^0, or an accumulation layer in the TiO_x conduction band depends on the mobility of counterions which are currently unidentified. In either case, the structural changes observable with Raman spectroscopy are those associated with NAB.

The smaller rectification with a 1.0 nm layer of Ti (Figure 11) or its complete absence with Cu substituted for Ti[32] indicates that rectification is not an inherent property of the NAB layer. However, linear, nonrectifying *i*/*V* curves with NAB absent (Figure 10) indicate that rectification results from a combination of NAB and TiO_x. With both TiO_x and NAB present, a carbon/molecule/semiconductor/metal junction results, with properties reflecting the junction structure in its entirety. One possible rectification mechanism is based on the energetics of the TiO_x conduction band and the NAB LUMO. Kuciauskas et al.[60] assign a conduction band energy for nanocrystalline TiO_2 of approximately −0.56 V vs NHE, and the $E_{1/2}$ for NAB/NAB^- chemisorbed on PPF is −0.54 V vs NHE.[55] For negative bias in $PPF/NAB/TiO_x/Au$ junctions, we expect NAB to be reduced and electrons to be removed from the TiO_x layer. Hence the TiO_x may be deficient of carriers in its conduction band, resulting in low junction conductivity. In addition, reduction of NAB will change the energies of its molecular orbitals and/or generate a coulomb barrier in the NAB layer. For positive bias, however, electrons are injected into TiO_x, generating carriers which may flow into the NAB LUMO and thus through the junction. The relative energies of the NAB LUMO and the TiO_x conduction band in the absence of electrolyte are estimates at best, but they do imply that rectification controlled by electron injection from Au to TiO_x to NAB is at least energetically feasible.

The insets in Figure 10 reinforce the hypothesis that positive bias results in oxidized NAB, and the resulting junction has high conductivity due to mobile electrons in TiO_x. As the bias is scanned negative rapidly (100 V/s for red curve), electrons are driven from TiO_x to NAB^-, and the junction conductivity decreases. This model postulates that junction conductivity depends on both the organic layer and TiO_x, and that the reversal of the applied bias causes changes in both layers. We proposed

(60) Kuciauskas, D.; Freund, M. S.; Gray, H. B.; Winkler, J. R.; Lewis, N. S. *J. Phys. Chem. B* **2001**, *105*, 392.

previously for NAB junctions with Hg top contacts that the quinoid NAB^- should be a better conductor due to its smaller HOMO−LUMO gap.[56,61] The current results do not contradict that proposal, provided the TiO_x layer has a larger effect on conductivity than the organic layer. The conductivity of the NAB/NAB^- layer may be the minority determinant of conductivity in PPF/NAB/TiO_x/Au junctions, but the organic layer does provide a source or sink of electrons necessary to modulate TiO_x conductivity. It should be noted that there is a precedent for oxide-mediated hysteresis from studies of electron tunneling, in which "switching" behavior in Cu/TCNQ/Al tunnel junctions was eventually attributed to formation of aluminum oxide upon exposure of the junctions to air.[62]

It is perhaps risky to use a redox cell model to explain structural changes in PPF/NAB/TiO_x/Au junctions, since such junctions have no intentional solvent or electrolyte, and no reference electrode to establish a potential scale. However, the predicted electric field in the junction ($>10^6$ V/cm) is of the same order of magnitude as electric fields in electrochemical double layers, so adequate driving force for a redox process is present. Assuming this high field can drive electrons into or out of the NAB/NAB^- layer, NAB molecules may respond by reorganization to accommodate injection or removal of electrons from the LUMO. Stated differently, the anionic quinoid form of NAB may be more stable in a high electric field than neutral NAB. The time required for reorganization of NAB may be responsible for the variations in conductance with scan rate apparent in Figure 9, and the hysteresis in Figure 10. Alternatively, it is possible that mass transport of adventitious ions (if present) accompanying a redox process may limit the rate at which the reaction can proceed.

In summary, the in situ Raman probe of NAB junctions has provided clear evidence for molecular structure changes in response to an applied electric field, which are both reproducible and repeatable. Although these changes are similar to those observed in an electrochemical cell, there is no known solvent or electrolyte present. In addition, it is clear that the rectification and conductance switching reported previously are dependent on both the NAB layer and the Ti/TiOx layer, since the absence of either layer results in symmetric *i*/*V* curves with no hysteresis. The spectroscopic changes observed are not explainable by metal filaments or "short circuits" through the molecular layer, unless such artifacts also produce molecular rearrangement in the NAB film. While the spectroscopic changes firmly establish the presence of chemical changes in the molecular junction in an applied field, the mechanism by which those changes modulate the junction conductance is less clear. Possibilities include (at least) injection of electrons into the conduction band of the titanium oxide, formation of metallic Ti or TiO, and changes in the NAB HOMO−LUMO gap. Current investigations seek to probe the conduction mechanism through its dependence on temperature, molecular structure, and the properties of the metal oxide.

Acknowledgment. This work was supported by the National Science Foundation through project 0211693 from the Analytical and Surface Chemistry Division, and by ZettaCore, Inc.

JA045763R

(61) Solak, A. O.; Eichorst, L. R.; Clark, W. J.; McCreery, R. L. *Anal. Chem.* **2003**, *75*, 296.
(62) Hoagland, J. J.; Wang, X. D.; Hipps, K. W. *Chem. Mater.* **1993**, *5*, 54.
(63) Biswas, N.; Umapathy, S. *J. Phys. Chem. A* **2000**, *104*, 2734.